

# Structural Interpretation of Metastable States in MbNO

Maksym Soloviov, Akshaya K. Das and Markus Meuwly\*

*Department of Chemistry, University of Basel,*

*Klingelbergstrasse 80, 4056 Basel, Switzerland*

E-mail: m.meuwly@unibas.ch

## Abstract

Nitric oxide binding and unbinding from myoglobin (Mb) is central to the function of the protein. Using reactive molecular dynamics (MD) simulations the dynamics following NO dissociation is characterized both, in time and in space. The time scales for ligand rebinding include two processes on the 10 ps and 100 ps time scale which agrees with recent optical and X-ray absorption experiments. Explicitly including the iron-out-of-plane (Fe-oop) coordinate is essential for meaningful interpretation of the data. Also, the proposed existence of an “Fe-oop/NO-bound” state is confirmed and assigned to NO at a distance of  $\approx 3 \text{ \AA}$  away from the iron atom. However, calculated XANES spectra suggest that it is difficult to distinguish between NO close but chemically unbound to the heme-Fe and positions further away in the primary site. Another elusive state, Fe-ON coordination, is not observed experimentally because it is masked by the energetically more favorable but dissociative  $^4A$  state in this region which makes the Fe-ON local minimum unobservable in wild type Mb. However, suitable active site mutations may stabilize this state.

---

\*To whom correspondence should be addressed

1  
2  
3  
4 Characterizing structure, motions and functional dynamics in biomolecules is essential for  
5  
6 understanding their function. The motions usually involve stable states at their endpoints,  
7  
8 separated by one or several metastable states (intermediates) in between.<sup>1,2</sup> Experimentally,  
9  
10 it is possible to directly and structurally characterize states with sufficiently long lifetimes.<sup>3,4</sup>  
11  
12 However, when the states live for times too short to stabilize only indirect means to infer  
13  
14 their existence are available. Optical spectroscopy can reveal the existence of short lived  
15  
16 states through spectral shifts. More direct interrogation of the chemical environment of the  
17  
18 iron atom is possible with X-ray absorption spectroscopy (XAS)<sup>5</sup> or multidimensional spec-  
19  
20 troscopy.<sup>6,7</sup> However, associating time scales with particular geometrical arrangements of the  
21  
22 atoms is usually indirect, except for favourable cases.<sup>4</sup> Under such circumstances computa-  
23  
24 tional investigations including the dynamics of the system of interest becomes a meaningful  
25  
26 complement.  
27  
28  
29  
30  
31

32 Following the motion of photodissociated ligands in globular proteins has a long history.  
33  
34 Small molecules which can reversibly bind to the protein active center are ideal and sensitive  
35  
36 probes of the interior of such complex systems. Nitric oxide (NO) is a physiologically relevant  
37  
38 ligand,<sup>8-10</sup> involved in modulating blood flow, thrombosis, and neural activity. Experimen-  
39  
40 tally, the binding kinetics of NO to the heme-group in myoglobin (Mb) has been studied  
41  
42 extensively with time resolved spectroscopies, ranging from UV/visible to the mid-IR<sup>11-17</sup>  
43  
44 and resonance Raman<sup>14</sup> techniques. In all cases the rebinding kinetics is multi-exponential  
45  
46 with time constants ranging from sub-picoseconds to several hundred picoseconds. However,  
47  
48 they can be grouped into two broad classes: processes on the 10 ps time scale and those on  
49  
50 the 100 ps time scale.<sup>12,14-16,18,19</sup>  
51  
52  
53  
54

55 Recent experiments have followed the interplay between the Fe-out-of-plane (Fe-oop) and  
56  
57 the NO-ligand motion in a time resolved fashion.<sup>5,14,16</sup> This work points towards a direct  
58  
59 coupling between these two degrees of freedom on the 10 to 100 ps time scale. What re-  
60  
61  
62  
63  
64  
65

1  
2  
3  
4 mains unclear is the structural characterization of this state. Furthermore, earlier studies  
5  
6 have attempted to characterize the metastable Fe-ON state<sup>20</sup> and the question remains why  
7  
8 this commonly observed motif in model compounds<sup>21</sup> is absent in the protein environment  
9  
10 despite a stabilization of 5 kcal/mol or more.<sup>22</sup>  
11  
12  
13

14  
15 The atomistic dynamics is essential for protein function and provides the basis to interpret  
16  
17 the time scales involved at a structural level. Molecular dynamics (MD) simulations are  
18  
19 ideal for addressing such questions. Together with validated energy functions such simula-  
20  
21 tions can provide the “missing link” between time resolved experiments and the underlying  
22  
23 atomic motions.<sup>4,23,24</sup> For NO interacting with heme in Mb such potential energy surfaces  
24  
25 (PESs) for the bound  ${}^2A$  and ligand-unbound  ${}^4A$  state are available.<sup>25</sup>  
26  
27  
28

29  
30 Running a statistically significant number of QM/MM trajectories from which to analyze  
31  
32 and resolve the interplay of the motions involved is beyond current computational methods  
33  
34 for systems such as MbNO. For quantitative and meaningful computational investigations,  
35  
36 suitable representations that preserve the accuracy of the interpolated PES are used in the  
37  
38 simulations. Here, a parameter-free, reproducing kernel Hilbert space (RKHS)-based repre-  
39  
40 sentation which exactly reproduces the reference data from quantum chemical calculations  
41  
42 is employed (for details on the PESs, see the SI).<sup>26,27</sup> RKHS is based on smoothness criteria  
43  
44 of the interpolant and has been successfully applied to study van der Waals complexes.<sup>28,29</sup>  
45  
46  
47

48  
49 The present work investigates the reactive dynamics between the  ${}^4A$  and  ${}^2A$  PESs following  
50  
51 photodissociation of the NO ligand from the heme-iron in Mb. Due to the close energetic  
52  
53 ordering of the two states and the existence of two substates on the  ${}^2A$  PES, interesting dy-  
54  
55 namics can be expected. From comparison with experimentally determined rebinding time  
56  
57 scales and the spectroscopies, structural questions underlying the molecular dynamics can  
58  
59 be addressed.  
60  
61  
62

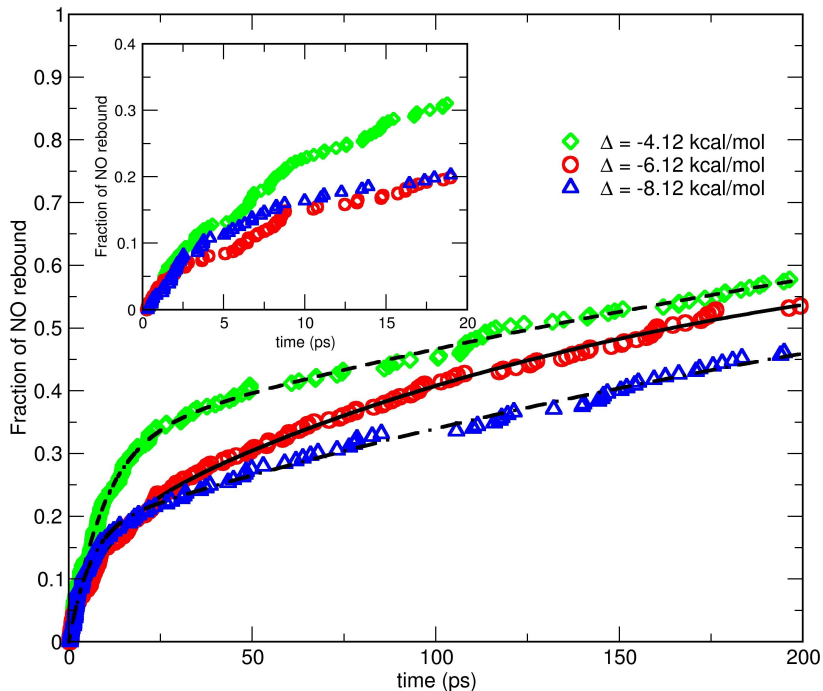


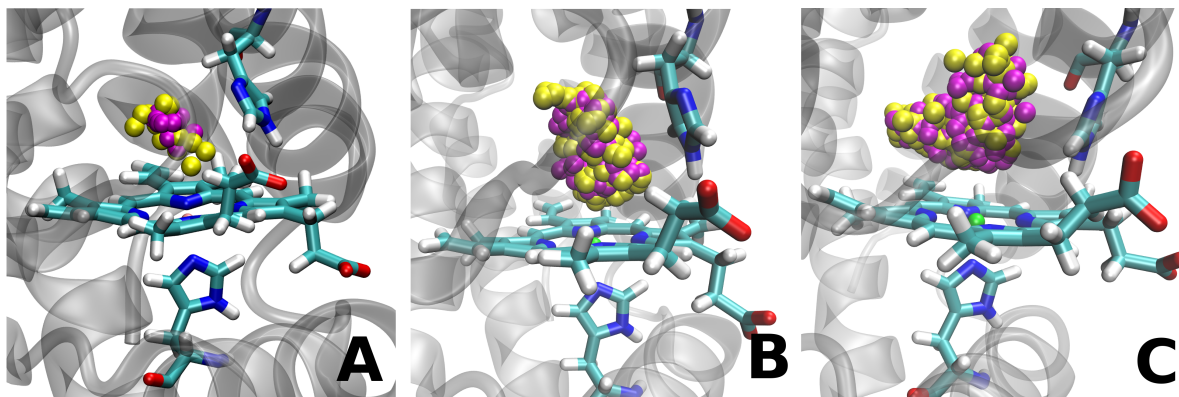
Figure 1: The kinetics and the corresponding exponential fits for NO rebinding to the heme-Fe after photoexcitation. Simulations were run for three different values of the asymptotic shift  $\Delta$ .

For following the reactive dynamics between the  $^2A$  and  $^4A$  states, 300 independent simulations were run for a maximum time of 200 ps or until the bound Fe-NO state was formed. Photodissociation was induced by instantaneously switching the force field to the  $^4A$  state<sup>30</sup> which introduces around 50 kcal/mol of energy,<sup>25</sup> comparable with the photon energies used in experiments (49 to 81 kcal/mol).<sup>31</sup> The rebinding kinetics is reported in Figure 1 and shows the fraction of rebound NO as a function of time. The rebinding kinetics on the sub-nanosecond time scale follows a multiexponential decay with two time constants  $\tau_1 \approx 10$  ps and  $\tau_2 \approx 150$  ps, also depending on the asymptotic separation  $\Delta$  of the two states (see Table I SI). The shift  $\Delta$  relates the asymptotic energies of the  $^2A$  and the  $^4A$  PESs for NO at infinite separation from the heme-Fe (see SI).

Typical ligand trajectories are shown in Figure 2. Panel A reports rebinding on the 1 ps time

1  
2  
3  
4 scale whereas panels B and C are representative of rebinding time scales  $\tau_1$  and  $\tau_2$ . For  $\tau_1$   
5  
6 the ligand only samples the immediate neighborhood of the heme-iron before rebinding. On  
7  
8 the 100 ps time scale rebinding occurs from regions further away. For  $\Delta = -6.1$  kcal/mol  
9  
10 the total number of rebound trajectories is 17 (rebinding within 2 ps), 28 ( $2 \leq t < 10$ ),  
11  
12 115 ( $10 \leq t < 200$ ), and 140 rebound on time scales longer than 200 ps, i.e. the rebinding  
13  
14 efficiency within 200 ps is  $\sim 55$  %. This compares with a rebound fraction of 75 % on the  
15  
16 200 ps time scale from recent XAS measurements.<sup>5</sup>  
17  
18  
19  
20

21 The simulations described so far used the PESs fitted to the DFT-data and including en-  
22  
23 vironmental effects (see SI). Corresponding simulations with 200 independent runs on the  
24  
25 DFT-only PESs yield rebinding of 195 trajectories within 200 ps with rebinding times of  
26  
27 2 and 15 ps, i.e. one order of magnitude more rapid than with the refined PES treating  
28  
29 the Fe-oop coordinate more accurately and explicitly. This finding is also consistent with  
30  
31 previous simulations based on DFT-only PESs.<sup>19,32</sup> Hence, explicitly including the Fe-oop  
32  
33 motion is essential for quantitative results.  
34  
35  
36  
37



52 Figure 2: Typical trajectories for different rebinding time scales. NO positions are shown  
53 in yellow (N) and magenta (O). (A) - the picosecond process ( $\tau = 1.6$  ps), (B) - the 10  
54 picosecond process ( $\tau = 42.1$  ps), (C) - the 100 picosecond process ( $\tau = 160.2$  ps).  
55  
56  
57

58 A complementary view of the different rebinding time scales can be gained from analyzing  
59 the maximal distance between the Fe and the ligand sampled during a rebinding simulation.  
60  
61  
62  
63  
64  
65

1  
2  
3  
4 The 300 trajectories were grouped in those that rebind on very short time scales ( $\tau < 2$  ps),  
5 within 10 ps and longer than 10 ps. The individually normalized probability distribution  
6 functions (pdfs) are shown in Figure S5 (see SI). No NO migration to neighboring xenon-  
7 binding sites is found on the 200 ps time scale because, e.g., escape to the closest Xe-site  
8 (Xe4) occurs within 1 to 10 ns.<sup>33,34</sup>  
9

10  
11  
12  
13  
14  
15  
16  
17 Previous experimental and computational investigations<sup>12,19,30,32,35-37</sup> found that the recom-  
18 bination kinetics of MbNO is non-exponential, involving two to three time scales, depending  
19 on the model used. The earliest works report time scales of 27.6 ps and 279.3 ps in a double  
20 exponential fit.<sup>12</sup> Later, optical and infrared experiments found short time scales ranging  
21 from 5 to 30 ps and longer time scales between 100 and 200 ps.<sup>35-37</sup> The experiments all  
22 agree on the existence of two sub-nanosecond time scales which differ by about one order of  
23 magnitude. Previous computations with reactive force fields find typically somewhat shorter  
24 rebinding times, between 5 ps and 20 ps,<sup>19,32</sup> depending on the asymptotic separation  $\Delta$   
25 used.<sup>38</sup> The current simulations find multiple time scales in the 10 to 100 ps range in agree-  
26 ment with optical and infrared experiments. Also, a more rapid component on the 1 to 2 ps  
27 time scale is present. The influence of Fe-doming is clearly visible in the rebinding kinetics,  
28 see Figure 1. This validates the force fields used here and allows to address a number of  
29 hypotheses put forward recently.  
30  
31  
32  
33  
34  
35  
36  
37  
38  
39  
40  
41  
42  
43  
44

45  
46 *The Fe-oop, NO-bound state:* First, direct contact with a recently proposed transient struc-  
47 ture in the  $^2A$  state can be made. Picosecond time resolved<sup>14</sup> and XAS<sup>5</sup> experiments have  
48 suggested that the Fe-out-of-plane (Fe-oop) and the NO-ligand motion are closely coupled.  
49 The interpretation of the experiments provided evidence for an Fe-oop, ligand bound struc-  
50 ture with a lifetime of  $30 \pm 10$  ps. The present simulations on the  $^2A$  PES alone indeed  
51 show transient stabilization of such a state. The maximal lifetime found was 27 ps and  
52 41.7 % of the trajectories showed such a state (see Figure S3). Despite underestimating the  
53  
54  
55  
56  
57  
58  
59  
60  
61  
62  
63  
64  
65

1  
2  
3  
4 experimentally reported lifetime of  $30 \pm 10$  ps the present simulations support the existence  
5  
6 of such a state.  
7  
8  
9

10 *The Fe-ON state:* Another structurally elusive state which has been found for heme-model  
11 compounds is the Fe-ON isomer.<sup>21,39,40</sup> Such a structure is sufficiently stabilized (by sev-  
12 eral kcal/mol) in NO-bound Mb which should make it observable in infrared experiments.<sup>22</sup>  
13  
14 However, no such state was found in experiments.<sup>20</sup> Simulations on the  ${}^2A$  state alone show  
15 that the ligand is stabilized for tens of picoseconds in the Fe-ON state. However, when using  
16 the reactive  ${}^2A + {}^4A$  PES with a shift of  $\Delta = -6.1$  kcal/mol (which best reproduces the  
17 DFT energies) the Fe-ON configuration can not be stabilized because in the region of the  
18 Fe-ON minimum the repulsive  ${}^4A$  state is lower in energy than the  ${}^2A$  state. Hence, the  
19  ${}^2A$  minimum of the Fe-ON state is masked by the  ${}^4A$  state and can not be stabilized in wt Mb.  
20  
21  
22  
23  
24  
25  
26  
27  
28  
29  
30

31  
32 The asymptotic separation  $\Delta$  depends on the chemical environment around the heme-group.  
33 Hence,  $\Delta$  changes if the environment is modified, e.g. through mutation of amino acids  
34 or embedding the heme-group into a different protein. The effect of this can be quantified  
35 with simulations on the reactive  ${}^2A + {}^4A$  PES with different values for  $\Delta$ . Reducing the  
36 asymptotic separation by 5 kcal/mol ( $\Delta = -11.1$  kcal/mol) further destabilizes the Fe-ON  
37 state (Figure SI 6A). For  $\Delta = -6.1$  kcal/mol (Figure SI 6B) the Fe-ON state is insignifi-  
38 cantly sampled and the system rebinds efficiently into the Fe-NO state. Contrary to that,  
39 reducing the asymptotic separation to  $\Delta = -1.1$  kcal/mol (Figure SI 6C) the Fe-ON state  
40 is populated for extended periods during which spectroscopic characterization of this state  
41 should be possible. As an illustration of this, recent spectroscopic work found a 2.5 times  
42 slower dynamics of NO rebinding in Mb compared to cytochrome c due to different active  
43 site architecture.<sup>41</sup> Based on transition state theory, a factor of 2.5 corresponds to  $\approx 0.5$   
44 kcal/mol in energy. The thermodynamic stability of Mb upon mutation has been found to  
45 change by  $-2$  to  $+6$  kcal/mol<sup>42</sup> which suggests that modifications in the active site can  
46  
47  
48  
49  
50  
51  
52  
53  
54  
55  
56  
57  
58  
59  
60  
61  
62  
63  
64  
65

1  
2  
3  
4 potentially stabilize the Fe–ON conformation through differential stabilization of the bound  
5 state relative to the unbound state.  
6  
7

8  
9  
10 *Structural interpretation of rebinding time scales:* With the coordinates from the reactive  
11 MD simulations it is possible to provide a structural interpretation of the  $\approx 10$  ps and  $\approx 100$   
12 ps time scale found in the rebinding simulations. It is of particular interest to investigate  
13 in what respect(s) the dynamics between these two states differ. Probability distribution  
14 functions of the a) NO-ligand, b) all active-site residues, and c) all His64 side chain atoms  
15 projected onto the heme plane are shown in Figure 3.  
16  
17  
18  
19  
20  
21  
22  
23  
24

25 The pdfs show that the NO-ligand explores a much larger space for long rebinding times  
26 (Figure 3 upper right hand panel) than for short rebinding times (Figure 3 upper left hand  
27 panel). Furthermore, the NE2 atom of residue His64 occupies two clearly distinguishable  
28 states (A and B) in trajectories with long rebinding times which are absent for rebinding  
29 on  $\tau_1 = 10$  ps (Figure 3 middle row). The middle row emphasizes that for time scales  $\tau_1$   
30 the His64 NE2 atom occupies space away from the iron (located at (0,0)) whereas for longer  
31 time scales the atom pushes in towards the heme-Fe by almost 2 Å which hinders ligand re-  
32 binding. The estimated forward  $\Delta G_{A \rightarrow B}^{\text{NE2}} = 2.5$  kcal/mol and reverse  $\Delta G_{B \rightarrow A}^{\text{NE2}} = 4.0$  kcal/mol  
33 barriers suggest that on the 100 ps time scale state A is destabilized relative to state B.  
34 Corresponding barrier heights for the other His64-side chain atoms range from 0.5 to 1.5  
35 kcal/mol. Hence, on average state B is separated from state A by a barrier of  $\approx 2$  kcal/mol  
36 with state B lower in energy than state A.  
37  
38  
39  
40  
41  
42  
43  
44  
45  
46  
47  
48  
49  
50

51  
52 The two states (A: green; B: red) are shown in Figure 4 together with the X-ray structure  
53 1HJT<sup>43</sup> (gold). State A (“His64 out”) is associated with the short rebinding time scale (10  
54 ps) whereas state B (“His64 in”) corresponds to the slow (100 ps) component. The barrier  
55 height corresponds to an interconversion time A $\leftrightarrow$ B on the sub-nanosecond time scale which  
56  
57  
58  
59  
60  
61  
62  
63  
64  
65

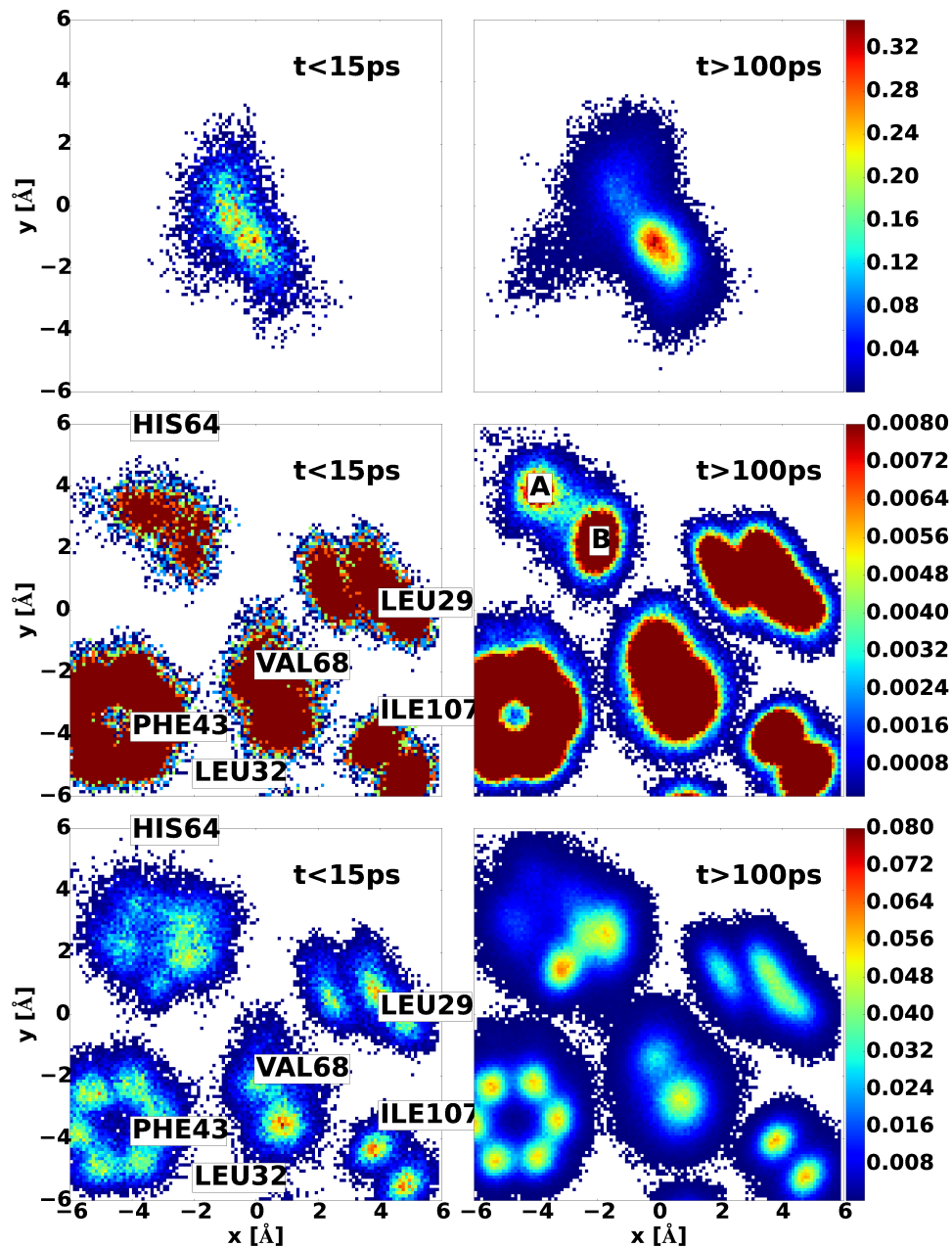
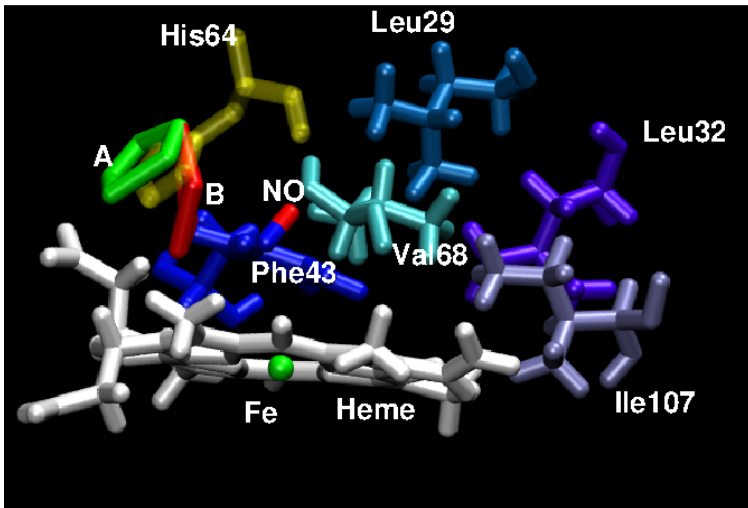


Figure 3: Top Panel:  $(x, y)$ -probability distribution function for the free NO ligand for rebinding on the  $t < 15$  ps (left) and  $t > 100$  ps (right) time scale. Middle Panel:  $(x, y)$ -probability distribution function for the NE2 atom of His64 on the two time scales. The two states for NE2 are labeled (A, B) and clearly distinguishable. Also shown are pdfs for all side chain atoms of Phe43, Val68, Leu29, and Ile107. For Phe43 the phenyl ring is always parallel to the heme-plane and all 6 carbon atoms are clearly distinguishable. Bottom Panel: as in the middle panel but for the entire side chain of His64 and with different maximum height of the pdfs.

1  
2  
3  
4 is supported by the explicit simulations and compares well with previous findings for CO-  
5 bound Mb with interconversion times of a few hundred picoseconds.<sup>6,44</sup>  
6  
7  
8  
9



10  
11  
12  
13  
14  
15  
16  
17  
18  
19  
20  
21  
22  
23  
24  
25  
26  
27  
28 Figure 4: States A (green) and B (red) as found from the per-atom pdfs of the His64-side  
29 chain atoms. In gold the X-ray reference structure.  
30  
31

32  
33 For direct contact with the XAS experiments, XANES spectra were computed (see SI) for  
34 randomly selected MD-sampled structures with NO-bound (40 structures), NO-unbound  
35 (NO within 3.5 Å of the heme-Fe; 20 structures) and NO-unbound (NO within 5.0 Å; 10  
36 structures). For the bound state the computed spectrum ( $I_b(E)$ ) agrees well up to 7.15 keV.  
37 For higher energies the absorption signal is correctly described but the computed intensity is  
38 too high (see Figure 5 top panel). The unbound structures yield  $I_{ub,s}$  and  $I_{ub,l}$  for the short  
39 and long Fe–NO separations, respectively, and nearly superimpose (inset Figure 5) despite  
40 the different NO separations. Upon ligand photodissociation the peak at 7.12 keV shifts  
41 to lower energy, the intensity between 7.12 and 7.15 keV decreases and between 7.15 and  
42 7.18 keV increases compared to the spectrum for the bound state. All these features are  
43 consistent with previous experiments on MbNO and deoxy-Mb.<sup>5,14</sup>  
44  
45  
46  
47  
48  
49  
50  
51  
52  
53  
54  
55  
56  
57

58 The experimentally observed transient at 50 ps is compared with the averaged absorbance  
59 differences  $\Delta I_{ub,s} = I_b - I_{ub,s}$  and  $\Delta I_{ub,l} = I_b - I_{ub,l}$  in Figure 5. The two computed difference  
60  
61  
62  
63  
64  
65

1  
2  
3  
4 spectra are quite similar - except for a slightly reduced amplitude around 7.13 keV and 7.15  
5 keV and an enhancement around 7.16 keV for  $\Delta I_{ub,s}$  compared to  $\Delta I_{ub,l}$  - despite the two  
6 very different ligand positions. In both cases the Fe-oop position ranges from 0.3 to 0.15 Å  
7 below the plane although for  $\Delta I_{ub,s}$  positions closer to in-plane ( $d = 0$ ) also occur. Compared  
8 to the experimental transient,  $\Delta I_{ub,s}$  and  $\Delta I_{ub,l}$  trace the major features but differ from it  
9 in the width of the 7.12 keV peak and the behaviour between 7.13 and 7.15 keV. Figure  
10 S7 (see SI) suggests that presence or absence of photodissociated NO affects the XANES  
11 spectrum over the entire energy range from 7.1 to 7.15 keV and not just around 7.15 keV as  
12 previously assumed<sup>5</sup> because the signal also depends on the motion of the Fe-atom relative  
13 to the heme-plane. Within the signal-to-noise of the experiment it can not be distinguished  
14 whether the ligand is close to the heme-Fe or further away from it. It should be recalled that  
15 experimentally, a mixture of NO-bound and NO-unbound structures is measured because  
16 the photolysis yield is not 100 %.

17  
18  
19  
20  
21  
22  
23  
24  
25  
26  
27  
28  
29  
30  
31  
32  
33  
34 Reactive MD simulations using MS-ARMD yield nonexponential kinetics for ligand rebind-  
35 ing. The time scales (10 and 100 ps) confirm those from optical and infrared experiments.  
36 The influence of the Fe-oop coordinate on the rebinding reaction has been directly estab-  
37 lished. The two time scales are associated with two structurally different states of the His64  
38 side chain - one “out” (state A) and one “in” (state B) - which control ligand access and  
39 rebinding dynamics. Although energetically feasible, the <sup>2</sup>A Fe-ON metastable state is likely  
40 to be unobservable in wild type Mb because in this region of configurational space the re-  
41 pulsive <sup>4</sup>A state is lower in energy and prevents stabilization. The present work supports a  
42 recently proposed, transient Fe-oop/NO-bound structure with lifetimes of up to 30 ps. The  
43 computed XAS spectra are compatible with experimentally measured ones but are unable  
44 to distinguish between structures with photodissociated NO “close to” or “far away” from  
45 the heme-Fe in the active site. The present work provides an atomistically refined picture  
46 and structural explanations and assignments for a range of experimental observations, all  
47  
48  
49  
50  
51  
52  
53  
54  
55  
56  
57  
58  
59  
60  
61  
62  
63  
64  
65

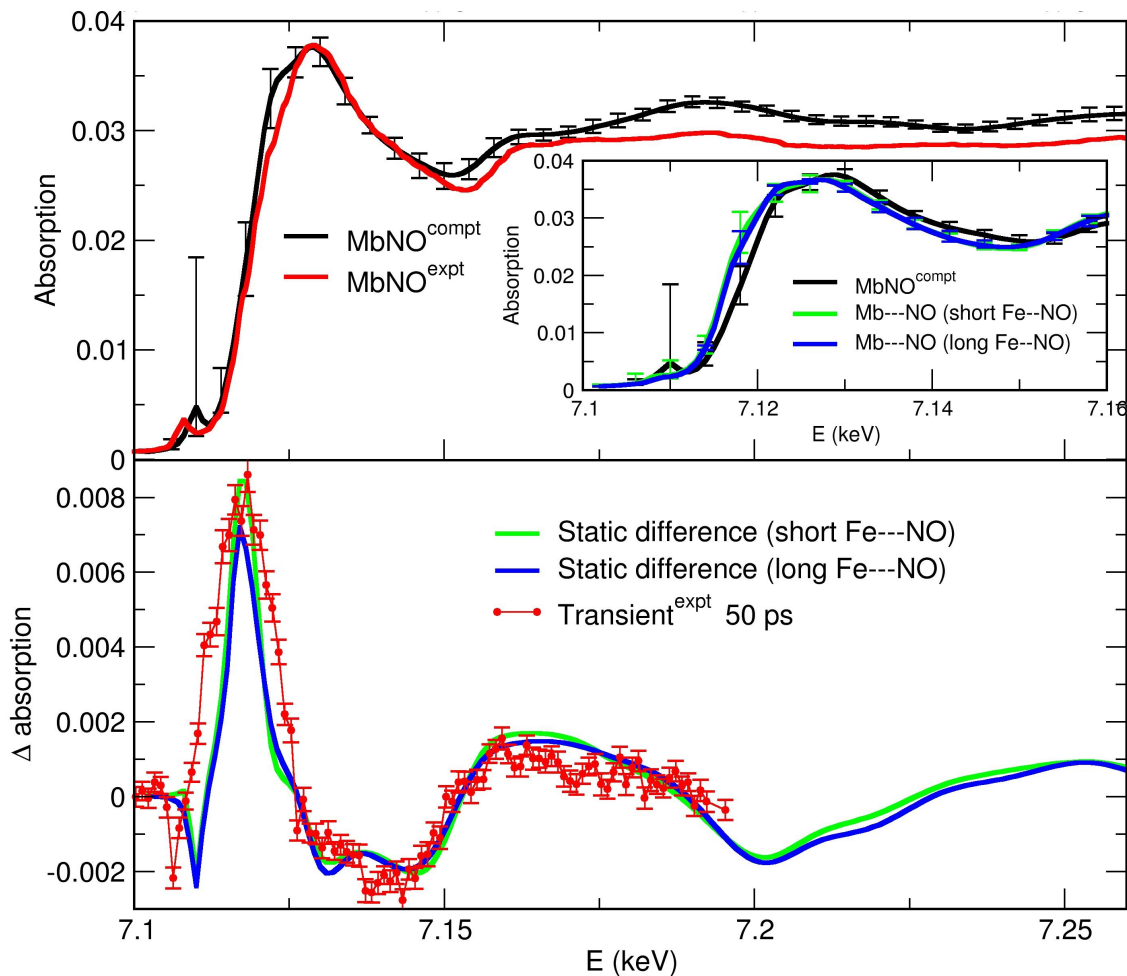


Figure 5: Top panel: Computed XANES spectra for MbNO (black) compared to experiment (red). Vertical bars indicate minimum and maximum absorption for all snapshots and are caused by conformational sampling. The inset compares computed spectra for MbNO and 2 sets of photodissociated systems (green and blue, see text). Bottom panel: Static difference spectra (green and blue) compared with the experimental transient at 50 ps (red).

sensitive to the Fe-oop dynamics of NO after photodissociation in native Mb.

## Acknowledgement

The authors acknowledge fruitful discussions with Chris Milne and helpful comments from Peter Hamm and Majed Chergui. This work was supported by the Swiss National Science Foundation through grants 200021-117810, and the NCCR MUST.

## References

- (1) Fischer, S.; Olsen, K. W.; Nam, K.; Karplus, M. *Proc. Natl. Acad. Sci.* **2011**, *108*, 5608–5613.
- (2) Menting, J. G. et al. *Proc. Natl. Acad. Sci.* **2014**, *111*, E3395–E3404.
- (3) Schlichting, I.; Berendzen, J.; Phillips, G.; Sweet, R. *Nature* **1994**, *371*, 808–812.
- (4) Schotte, F.; Lim, M.; Jackson, T. A.; Smirnov, A. V.; Soman, J.; Olson, J. S.; Phillips, G. N.; Wulff, M.; Anfinrud, P. A. *Science (New York, N.Y.)* **2003**, *300*, 1944.
- (5) Silatani, M.; Lima, F. A.; Penfold, T. J.; Rittman, J.; Reinhard, M.; Rittmann-Frank, H.; Borca, C.; Grolimund, D.; Milne, C. J.; Chergui, M. *Proc. Natl. Acad. Sci.* **2015**, *112*, 12922 – 12927.
- (6) Merchant, K. A.; Noid, W. G.; Thompson, D. E.; Akiyama, R.; Loring, R. F.; Fayer, M. D. *J. Phys. Chem. B* **2003**, *107*, 4–7.
- (7) Bredenbeck, J.; Helbing, J.; Nienhaus, K.; Nienhaus, G. U.; Hamm, P. *Proc. Natl. Acad. Sci.* **2007**, *104*, 14243–14248.
- (8) Pacher, P.; Beckman, J. S.; Liaudet, L. *Physiol. Rev.* **2007**, *87*, 315–424.
- (9) Lundberg, J. O. et al. *Nat. Chem. Biol.* **2009**, *5*, 865–869.
- (10) Traylor, T.; Sharma, V. *Biochem.* **1992**, *31*, 2847–2849.
- (11) Cornelius, P.; Hochstrasser, R.; Steele, A. *J. Mol. Biol.* **1983**, *163*, 119–128.
- (12) Petrich, J. W.; Lambry, J. C.; Kuczera, K.; Karplus, M.; Poyart, C.; Martin, J. L. *Biochem.* **1991**, *30*, 3975.
- (13) Ionascu, D.; Gruia, F.; Ye, X.; Yu, A.; Rosca, F.; Demidov, C. B. A.; Olson, J. S.; Champion, P. M. *J. Am. Chem. Soc.* **2005**, *127*, 16921–16934.

- 1  
2  
3  
4 (14) Kruglik, S. G.; Yoo, B.-K.; Franzen, S.; Vos, M. H.; Martin, J.-L.; Negreterie, M. *Proc.*  
5  
6 *Natl. Acad. Sci.* **2010**, *107*, 13678.  
7  
8  
9 (15) Kim, J.; Park, J.; Lee, T.; Lim, M. *J. Phys. Chem. B* **2012**, *116*, 13663–13671.  
10  
11  
12 (16) Yoo, B.-K.; Kruglik, S. G.; Lamarre, I.; Martin, J.-L.; Negreterie, M. *J. Phys. Chem. B*  
13  
14 **2012**, *116*, 4106–4114.  
15  
16  
17 (17) Kim, S.; Jin, G.; Lim, M. *J. Phys. Chem. B* **2004**, *108*, 20366.  
18  
19  
20 (18) Nutt, D. R.; Meuwly, M. *Biophys. J.* **2006**, *90*, 1191.  
21  
22  
23 (19) Danielsson, J.; Meuwly, M. *J. Chem. Theo. Comp.* **2008**, *4*, 1083.  
24  
25  
26 (20) Nienhaus, K.; Palladino, P.; Nienhaus, G. U. *Biochem.* **2008**, *47*, 935.  
27  
28  
29 (21) Xu, N.; Yi, J.; Richter-Addo, G. B. *Inorg. Chem.* **2010**, *49*, 6253–6266.  
30  
31  
32 (22) Nutt, D. R.; Karplus, M.; Meuwly, M. *J. Phys. Chem. B* **2005**, *109*, 21118.  
33  
34  
35 (23) Nutt, D. R.; Meuwly, M. *Proc. Natl. Acad. Sci.* **2004**, *101*, 5998.  
36  
37  
38 (24) Lee, M. W.; Carr, J. K.; Göllner, M.; Hamm, P.; Meuwly, M. *J. Chem. Phys.* **2013**,  
39  
40 *139*, 054506.  
41  
42  
43 (25) Soloviov, M.; Meuwly, M. *J. Chem. Phys.* **2015**, *143*.  
44  
45  
46 (26) Aronszajn, N. *Trans. Amer. Math. Soc.* **1950**, *68*, 337.  
47  
48  
49 (27) Hollebeek, T.; Ho, T. S.; Rabitz, H. *Ann. Rev. Phys. Chem.* **1999**, *50*, 537.  
50  
51  
52 (28) Ho, T. S.; Rabitz, H. *J. Chem. Phys.* **1996**, *104*, 2584.  
53  
54  
55 (29) Meuwly, M.; Hutson, J. M. *J. Chem. Phys.* **1999**, *110*, 8338.  
56  
57  
58 (30) Meuwly, M.; Becker, O. M.; Stote, R.; Karplus, M. *Biophys. Chem.* **2002**, *98*, 183–207.  
59  
60  
61  
62  
63  
64  
65

- 1  
2  
3  
4 (31) Lim, M.; Jackson, T. A.; Anfinrud, P. A. *Proc. Natl. Acad. Sci.* **1993**, *90*, 5801.  
5  
6  
7 (32) Nutt, D. R.; Meuwly, M. *Biophys. J.* **2006**, *90*, 1191–1201.  
8  
9  
10 (33) Bossa, C.; Anselmi, M.; Roccatano, D.; Amadei, A.; Vallone, B.; Brunori, M.; Di  
11 Nola, A. *Biophys. J.* **2004**, *86*, 3855.  
12  
13  
14  
15 (34) Plattner, N.; Meuwly, M. *Biophys. J.* **2012**, *102*, 333.  
16  
17  
18 (35) Kholodenko, Y.; Gooding, E.; Dou, Y.; Ikeda-Saito, M.; Hochstrasser, R. *Biochem.*  
19 **1999**, *38*, 5918–5924.  
20  
21  
22  
23 (36) Ye, X.; Demidov, A.; Champion, P. *J. Am. Chem. Soc.* **2002**, *124*, 5914–5924.  
24  
25  
26 (37) Kim, S.; Jin, G.; Lim, M. *J. Phys. Chem. B* **2004**, *108*, 20366–20375.  
27  
28  
29 (38) Banushkina, P.; Meuwly, M. *J. Chem. Phys.* **2007**, *127*.  
30  
31  
32 (39) Carducci, M.; Pressprich, M.; Coppens, P. *J. Am. Chem. Soc.* **1997**, *119*, 2669–2678.  
33  
34  
35 (40) Cheng, L.; Novozhilova, I.; Kim, C.; Kovalevsky, A.; Bagley, K. A.; Coppens, P.;  
36 Richter-Addo, G. B. *J. Am. Chem. Soc.* **2000**, *122*, 7142.  
37  
38  
39 (41) Hunt, N. T.; Greetham, G. M.; Towrie, M.; Parker, A. W.; Tucker, N. P. *Biochem. J.*  
40 **2011**, *433*, 459–468.  
41  
42  
43  
44 (42) Kepp, K. P. *Bioch. Bioph. Acta* **2015**, *1854*, 1239–1248.  
45  
46  
47 (43) Brucker, E. A.; Olson, J. S.; Ikeda-Saito, M.; Phillips, G. N. *Prot. Struct. Funct. Genet.*  
48 **1998**, *30*, 352.  
49  
50  
51  
52 (44) Ma, J.; Huo, S.; Straub, J. *J. Am. Chem. Soc.* **1997**, *119*, 2541–2551.  
53  
54  
55  
56  
57  
58  
59  
60  
61  
62  
63  
64  
65